



Full length article

Inheritance from glass to liquid: β relaxation depresses the nucleation of crystals

L.J. Song^{a,b}, M. Gao^c, W. Xu^{a,b}, J.T. Huo^{a,b,*}, J.Q. Wang^{a,b,d,*}, R.W. Li^{a,b}, W.H. Wang^e, J.H. Perepezko^c

^a Key Laboratory of Magnetic Materials and Devices, and Zhejiang Province Key Laboratory of Magnetic Materials and Application Technology, Ningbo Institute of Materials Technology and Engineering, Chinese Academy of Sciences, Ningbo 315201, China

^b Center of Materials Science and Optoelectronics Engineering, University of Chinese Academy of Sciences, Beijing 100049, China

^c Department of Materials Science and Engineering, University of Wisconsin-Madison, Madison, WI 53706, USA

^d School of Materials Science and Engineering, Zhengzhou University, Zhengzhou 450001, Henan, China

^e Institute of Physics, Chinese Academy of Science, Beijing 100190, China

ARTICLE INFO

Article history:

Received 2 May 2019

Revised 1 October 2019

Accepted 1 December 2019

Available online 3 December 2019

Keywords:

Metallic glass

Relaxation

Crystallization

Nucleation rate

Quenched-in cluster

ABSTRACT

Both crystallization and relaxation are intrinsic characteristics that derive from the metastable nature of metallic glasses. However, the interactions between the two reactions are not understood fully. In this paper, enthalpy evolution and phase existence diagrams composed of liquid, glass and crystal are established to illustrate the phase transitions upon heating and cooling a metallic glass-forming material. We find that metallic glasses located in different enthalpy levels in the diagrams exhibit quite different resistance to crystallization. The crystal nucleation rate for the fast-cooled glass is smaller compared to the slow-cooled glass, which is verified to be correlated with the larger amount of β relaxation in the fast-cooled sample. These findings provide new evidence for the inheritance between glass and liquid, and suggest that modulating the glassy state is a new route to control the crystallization kinetics of supercooled liquids.

© 2019 Acta Materialia Inc. Published by Elsevier Ltd. All rights reserved.

1. Introduction

Crystallization represents the first-order phase transition from a disordered structure to an ordered structure. The frustration of crystallization leads to formation of glass when a melt is cooled fast enough. Bulk metallic glasses have promising application potentials as structural and functional materials and are ideal model materials for scientific researches [1–6]. It is intriguing that the proper crystallization of metallic glasses can enhance their properties, e.g. mechanical properties [7,8], magnetic properties [9] and catalytic activity [10,11]. However, understanding and controlling the crystallization behavior remain a challenge in materials science and condensed matter physics [12–15]. Crystallization is composed of two steps, i.e. nucleation of crystals and subsequent growth [16]. An asymmetric crystallization behavior has been found during cooling and heating processes [17,18]. In metallic glasses usually

higher rates are required to suppress crystallization when heating from a low-temperature glassy state compared to cooling from a high-temperature melt [19,20]. However, it is still not clear how the glassy state influences the crystallization kinetics of supercooled liquids. Unraveling the underlying mechanisms is essential for controlling the crystallization of supercooled liquids and for promoting the applications of metallic glasses.

The glass may reside in very large energy range with complex energy states according to the energy landscape theory. The energy changes along with the thermal history owing to the non-equilibrium nature of glasses. For example, when a glass is cooled slowly or annealed at elevated temperatures, the glass relaxes towards lower energy states. The relaxation plays an important role in influencing the properties of metallic glasses, e.g. mechanical properties and magnetic properties [21–23]. The relaxation processes for glasses usually exhibit diverse kinetics. For example, a glass may experience the Boson peak, fast-process, β relaxation and α relaxation successively when it is heated from low temperatures [21]. Metallic glasses also experience multiple relaxation stages when they are annealed isothermally close to the glass transition temperature [24–26]. Given the strong inheritance and memory effects in the metallic glasses and their supercooled liquids, an understanding of the influence of the diverse relaxation

* Corresponding authors at: Key Laboratory of Magnetic Materials and Devices, and Zhejiang Province Key Laboratory of Magnetic Materials and Application Technology, Ningbo Institute of Materials Technology and Engineering, Chinese Academy of Sciences, Ningbo 315201, China.

E-mail addresses: huojuntao@nimte.ac.cn (J.T. Huo), jqwang@nimte.ac.cn (J.Q. Wang).

modes in metallic glasses on the crystallization behavior of supercooled liquids is essential for establishing a control of the reaction kinetics.

The Flash differential scanning calorimeter (F-DSC) with high precision and high heating/cooling rates is capable of detecting the fine scale relaxation changes in glasses and the fast metastable phase transition phenomena [27–30]. The β relaxation and α relaxation can be distinguished by measuring the details of the enthalpy evolution during isothermal annealing by using F-DSC [24]. Thus, the F-DSC enables the determination of any correlations between the relaxation modes in metallic glasses and the crystallization behavior of supercooled liquids.

In this work, the correlation between the relaxation behavior and crystallization characteristics was studied using F-DSC in a model metallic glass with composition of $\text{Au}_{49}\text{Cu}_{26.9}\text{Ag}_{5.5}\text{Pd}_{2.3}\text{Si}_{16.3}$ [20,24,29,31]. Phase formation diagrams composed of glass, crystal and liquid phases are constructed to illustrate the competition between crystallization and glass transition upon cooling and heating. The correlations between the crystallization in supercooled liquids and the relaxation in glassy state are studied for metallic glasses in different energy states.

2. Methods

2.1. Sample preparation

An alloy with nominal composition of $\text{Au}_{49}\text{Cu}_{26.9}\text{Ag}_{5.5}\text{Pd}_{2.3}\text{Si}_{16.3}$ (at%) was prepared by arc melting the pure elements (>99.9 wt%) under the protection of high-purity Ar gas. The alloy was then remelted in a quartz tube and injected on a fast spinning copper roller at the wheel speed 40 m/s. The thickness of the metallic glass ribbons are about 30 μm .

2.2. F-DSC measurements

The thermal properties were measured using an F-DSC (Flash DSC 1 by Mettler Toledo). A tiny sample with dimensions of about $80\ \mu\text{m} \times 80\ \mu\text{m} \times 30\ \mu\text{m}$ was cut from a melt-spun ribbon. The sample was then loaded on the center of the F-DSC sensor chip under an optical microscope. In measurements, the sensor and the sample were protected from oxygen and moisture under a steady Ar flow (60 ml/min). The sample was first melted by heating up to 693 K at 1000 K/s and held isothermally for 5 min to allow the melt to contact well with the chip sensor. A second heating was done at 1000 K/s to determine the melting temperature ($T_m = 611\ \text{K}$). The liquidus temperature is determined to be $T_l = 660\ \text{K}$ using a conventional DSC (see the data in Fig. S1). The cooling rates range from 100 K/s to 10,000 K/s, and the heating rates range from 50 K/s to 40,000 K/s. Since the melting enthalpy is $\Delta H = 45.0\ \text{J/g}$ ($= 5.2 \times 10^8\ \text{J/m}^3$) and the fusion enthalpy of the F-DSC sample is about 30.6 μJ , the mass of the flash DSC sample is determined to be about 0.68 μg . The crystallization fraction of the sample was evaluated by the melting enthalpy because of their linear relationship. To measure the Time-Temperature-Transformation (TTT) curve, the metallic glass was heated (at a rate of 40,000 K/s) to a destination temperature and annealed isothermally. An exothermic peak is detected upon crystallization and the peak onset gives the crystallization onset time during isothermal annealing.

2.3. Microstructure characterization

The F-DSC samples were removed from the calorimetry chip and fabricated by a focused ion beam (FIB, Auriga by Carl Zeiss) to prepare a transmission electron microscope (TEM) sample for observation. The microstructure of the as-cooled and crystallized metallic glasses was studied in a Talos F200X TEM (by ThermoFisher).

3. Results

3.1. The phase formation diagrams upon cooling and heating

Fig. 1(a) shows the representative heat flow traces upon cooling at various cooling rates (R_{cool}). During slow cooling (e.g. $R_{\text{cool}} \leq 800\ \text{K/s}$), the liquid solidifies into crystals at a temperature T_{solid} . The T_{solid} decreases with increasing cooling rate. This is a typical kinetic characteristic of crystallization. When the cooling rate is larger than a critical value, R_c (i.e. $R_{\text{cool}} \geq 1600\ \text{K/s}$), the melt can be supercooled until it is frozen into a glass at a temperature $T_{g,c}$. The liquid-to-glass transition is accompanied by a heat capacity inflection at $T_{g,c}$, as shown in Fig. 1(a). To illustrate the competition of the crystal formation and glass formation, a phase existence region diagram in form of temperature versus cooling rate is shown in Fig. 1(b). The critical cooling rate for glass formation is determined to be about 1600 K/s. It is interesting to note that the T_{solid} exhibits a much stronger dependence on cooling rate compared to the $T_{g,c}$.

The representative heating F-DSC traces for metallic glasses cooled at different rates are shown in Fig. 1(c). If the liquid crystallizes at low cooling rates (i.e. $R_{\text{cool}} \leq 800\ \text{K/s}$), a melting reaction is detected upon heating. If the liquid is frozen into a metallic glass (i.e. $R_{\text{cool}} \geq 1600\ \text{K/s}$), the glass-to-liquid transition temperature (T_g), crystallization temperature (T_x) and melting temperature (T_m) are detected upon heating. Fig. 1(d) shows the 2-dimensional diagram of enthalpy evolution in terms of temperature and cooling rate based on the data in Fig. 1(c). At low cooling rates ($< 800\ \text{K/s}$), only the melting peak was detected without the glass transition and crystallization. This confirms that the sample crystallized completely during cooling. When the cooling rate is between 800 K/s and 1600 K/s, a glass-crystal composite is formed. If the cooling rate is above 1600 K/s, a fully amorphous structure is formed upon cooling.

The cooling rate is an effective parameter to modulate the energy states of glasses. To study the evolution of the enthalpy for metallic glasses cooled at different rates, the variation of F-DSC heat flows is obtained by subtracting the heat flow of the sample cooled at 1600 K/s, as shown in Fig. 1(e) (see details in Fig. S2). The enthalpy change is calculated by integrating the heat flow peak, $\Delta H = \int_{T_1}^{T_2} C_p dT$, with $T_1 = 330\ \text{K}$ is the integral lower limit that is below the relaxation peak, $T_2 = 460\ \text{K}$ is the integral upper limit that is above the relaxation peak, and C_p is the specific heat. As shown in Fig. 1(f), the enthalpy increases with the increase of the cooling rate.

The phase transition kinetics upon heating are studied by measuring the DSC traces at various heating rates, as shown in Fig. 2(a). At low heating rate (e.g. 1000 K/s), the metallic glasses experience the glass-to-liquid transition, crystallization and melting. The T_g and T_x of supercooled liquid shift to higher temperatures at higher heating rate (R_h). When T_x gets close to the melting temperature, crystallization gets frustrated because the crystallization driving force $\Delta H(T_l - T)/T_l$ (T is temperature, T_l is the liquidus temperature, ΔH is crystal melting enthalpy) becomes very small. The crystallization can be suppressed completely when R_h reaches about 10,000 K/s. The phase existence region diagram in Fig. 2(b) is shown to illustrate the phase transitions detected in Fig. 1(a). At low heating rates, the sample experiences glass, supercooled liquid, crystal and normal liquid states successively upon heating. At high enough heating rates, the glass transforms into supercooled liquid state and then normal liquid without crystallization. It is interesting that the phase transition onset temperatures, i.e., T_g and T_x , change in similar behavior for the glasses cooled at different rates. However, the critical heating rate where crystallization is depressed varies for the glasses cooled at different rates.

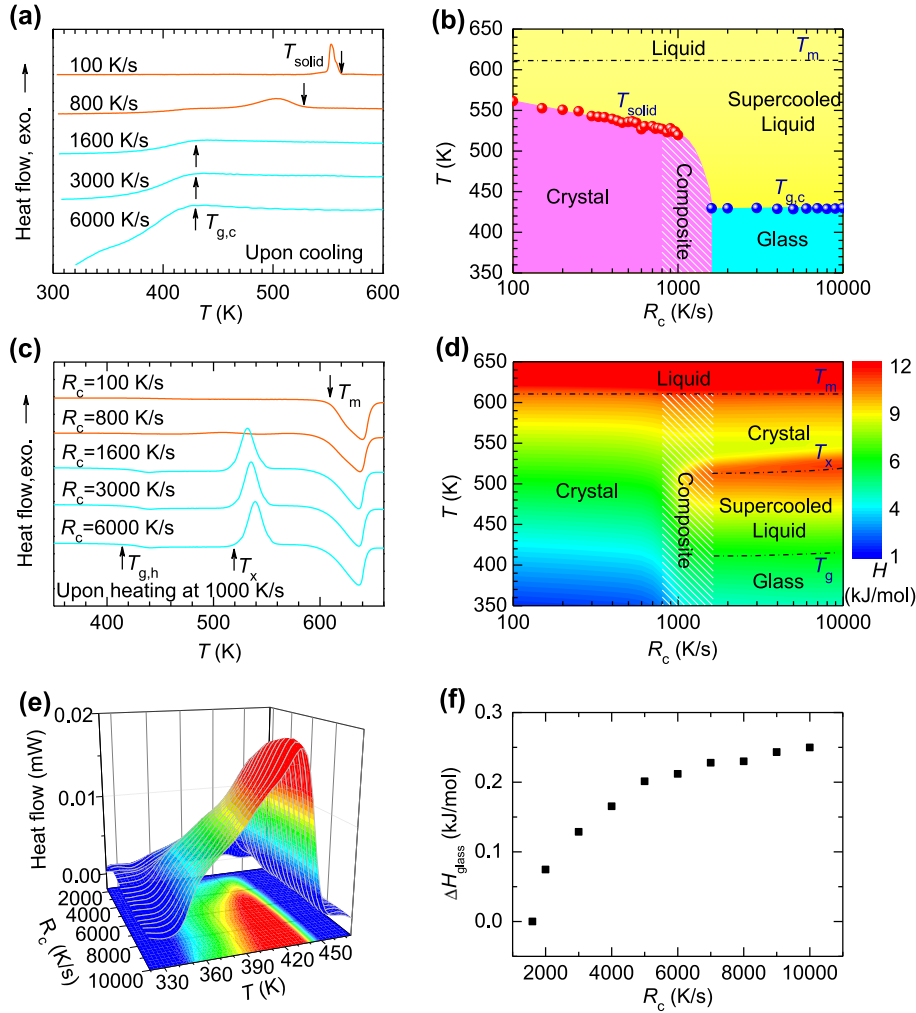


Fig. 1. Phase formation diagrams upon cooling. (a) The heat flows upon cooling at different rates. At low cooling rates, e.g. ≤ 800 K/s, the melt crystallizes. At high cooling rate, e.g. ≥ 1600 K/s, the melt transforms into glass. The onset temperatures for solidification (T_{solid}) and glass transition ($T_{\text{g,c}}$) are marked by arrows. (b) A phase existence region diagram in a form of temperature versus cooling rate (R_c) illustrating the formation of crystal and glass upon cooling a liquid. (c) The FDSC traces upon heating at 1000 K/s for samples cooled at different rates. The onset temperatures for glass transition (T_g), crystallization (T_x) and melting (T_m) are marked by arrows. The curves in (a) and (c) are shifted vertically by a constant to distinguish each other. (d) The 2-dimensional contours of the enthalpy in dimensions of temperature and cooling rate. (e) The 3-dimensional plot of heat flows upon subsequent heating ($R_h=1000$ K/s) versus cooling rate and temperatures. (f) The enthalpy of glassy state ΔH_{glass} relative to the enthalpy of the glass cooled at 1600 K/s as a function of cooling rate. ΔH_{glass} is obtained by integrating the rejuvenation heat flows peaks in (e).

Fig. 2(c) shows the crystallization fraction (X) upon heating versus the heating rate. Along with increasing the heating rate, the crystallization fraction is very sensitive to the cooling rates employed for glass synthesis. Crystallization of the fast-cooled glass exhibits a more sensitive dependence on heating rate, and the crystallization can be suppressed completely at a much lower heating rate compared to the slowly-cooled samples. To quantitatively study the crystallization kinetics upon heating, the crystallization fraction is fitted by a compressed exponential equation, as shown by the solid curves in Fig. 2(c).

$$X = \exp\left(-\left(\frac{R_h}{R_0}\right)^n\right) \quad (2)$$

where R_0 represents the heating rate where X reaches $1/e$, n is the exponent. As shown in Fig. 2(d), n increases from 1.8 to 2.31 and R_0 decreases from 4350 K/s to 2360 K/s when the cooling rate increases from 1600 K/s to 10,000 K/s. Values of $n > 1$ are attributed to the heterogeneous dynamics scenarios [25,32,33]. A larger n for the fast-cooled metallic glass in a high energy state suggests a strong heterogeneous nature.

3.2. Structural characterization

The microstructures of the metallic glasses that were slightly crystallized at the crystallization onset temperature were studied by TEM, as shown in Fig. 3 (the thermal protocols can be found in the Supplementary Fig. S4). A greater number of nanocrystals, N_a are developed in the metallic glass cooled at 1600 K/s compared to the metallic glass cooled at 10,000 K/s. The number density of nanocrystals is about 4.8 times different, which is consistent with the calculated N_a (3.5 times difference, see Supplementary Information). For the sample cooled at 1600 K/s, the nanocrystals in the sample cooled at 1600 K/s are more prone to nucleate on a dark catalyst as shown in Fig. 3(b) compared to the sample cooled at 10,000 K/s, which suggests more heterogeneous-like nucleation for the 1600 K/s cooled sample. This is consistent with the theoretical nucleation analysis (see Supplementary Information) that indicates that the catalytic potency factor, $f(\theta)$ for the sample cooled at 1600 K/s is larger than that for the metallic glass cooled at 10,000 K/s. The elemental mapping in Fig. 3(h) and the SAED patterns in Fig. 3(c) and (g) suggest that the nanocrystals are the AuCu phase [34] (details can be found in Supplementary Table S2).

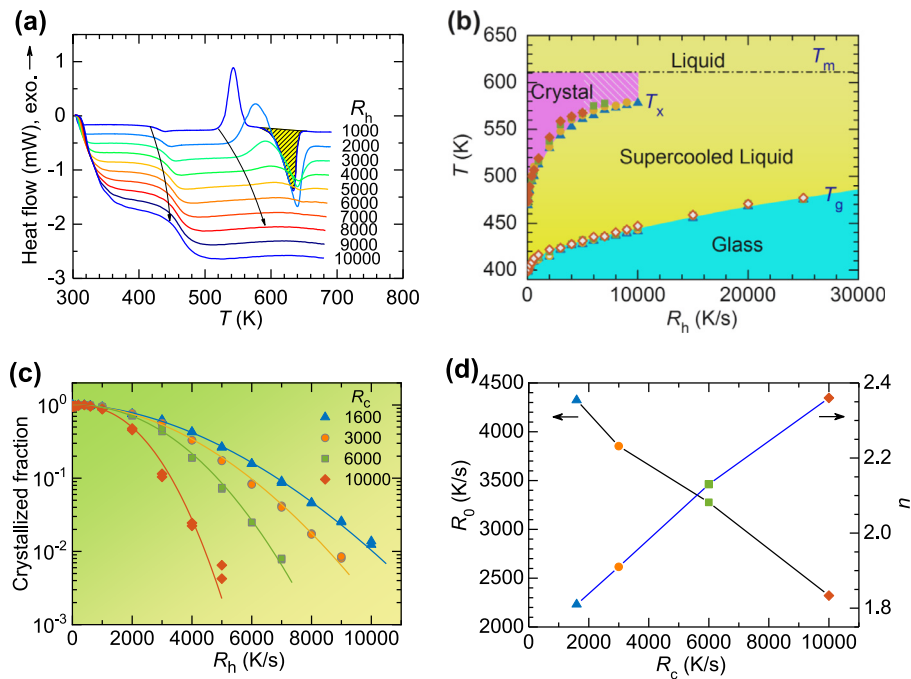


Fig. 2. Phase transitions upon heating. (a) Representative DSC traces for samples heated at various heating rates (from 1000 K/s to 10,000 K/s) for the metallic glass cooled at 10,000 K/s. (b) The phase existence region diagram upon heating a glass. Blue triangles: glass cooled at 1600 K/s. Yellow circles: glass cooled at 3000 K/s. Green squares: glass cooled at 6000 K/s. Red diamonds: glass cooled at 10,000 K/s. Filled symbols: crystallization temperature T_x . Open symbols: glass transition temperature T_g . (c) The heating rate (R_h) dependent crystallization fraction for the as-cooled samples cooled at different rates, 1600 K/s (triangles), 3000 K/s (circles), 6000 K/s (squares) and 10,000 K/s (diamonds), respectively. (d) The fitting parameters R_0 and n evolve with the cooling rate.

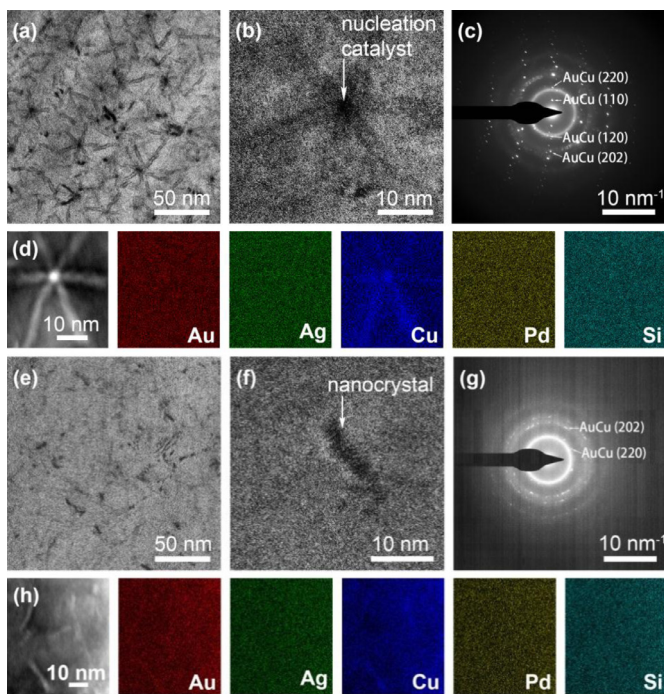


Fig. 3. The microstructure for the metallic glasses cooled from the crystallization onset temperatures. (a) The TEM image for the 1600 K/s cooled sample crystallized at 393 K. (b) The HRTEM image for nanocrystals that nucleate on a dark catalyst. (c) The selected area electron diffraction pattern shows a polycrystalline nature. (d) HAADF image of the nanocrystal and corresponding elemental mapping. (e) The TEM image for the 10,000 K/s cooled sample crystallized at 393 K. (f) The HRTEM image for a nanocrystal. (g) The selected area electron diffraction pattern shows a random nanocrystalline structure. (h) HAADF image of nanocrystal and corresponding elemental mapping.

3.3. Effects of β relaxation on the crystallization process of sample

The key difference between the metallic glasses cooled at different rates is the change in enthalpy states. It has been demonstrated that the change of glass enthalpy derives from different relaxation modes [24,35] so that monitoring the glass enthalpy can be used to distinguish between the different relaxation modes. Fig. 4(a) shows the representative DSC traces ($R_h=1500$ K/s) for the relaxed samples after annealing at 383 K for various times. With the increase of annealing time, both the relaxation peak (ΔH_g , the overshoot near T_g) and the crystallization peak (ΔH_x) become more pronounced. The relaxation kinetic barrier (ΔE) is determined using the Kissinger method (see Figs. S5 and S6). Fig. 4(b) shows the evolution of ΔE with the increase of annealing time. At the beginning, the ΔE is small and is equal to the value for β relaxation ($\sim 26RT_g$). With further annealing, the ΔE increases and reaches the value for α relaxation, which is consistent with previous work [24]. For comparison, the evolution of the crystallization enthalpy ΔH_x during the annealing is shown in Fig. 4(c). During the β relaxation stage, the ΔH_x is small and doesn't change much. When the β relaxation transforms to α relaxation, the crystallization enthalpy increases from 17.8 kJ/mol to 21.5 kJ/mol (also see Figs. S7 and S8). A 3D plot for ΔE versus ΔH_g and ΔH_x can be found in Fig. S8(b). The accelerated crystallization behavior is attributed to the activation of heterogeneous nucleation and crystallization [36]. These results suggest that the crystal nucleation can be suppressed in the supercooled liquid for the metallic glass that exhibits substantial β relaxation.

In Fig. 5(a) the evolution of the glass enthalpy at 383 K versus the relaxation barrier is shown and compared to the difference between the fast-cooled ($R_c=10,000$ K/s) and slow-cooled ($R_c=1600$ K/s) metallic glass. The y-axis is the excess enthalpy relative to the equilibrium supercooled liquid state. During the β

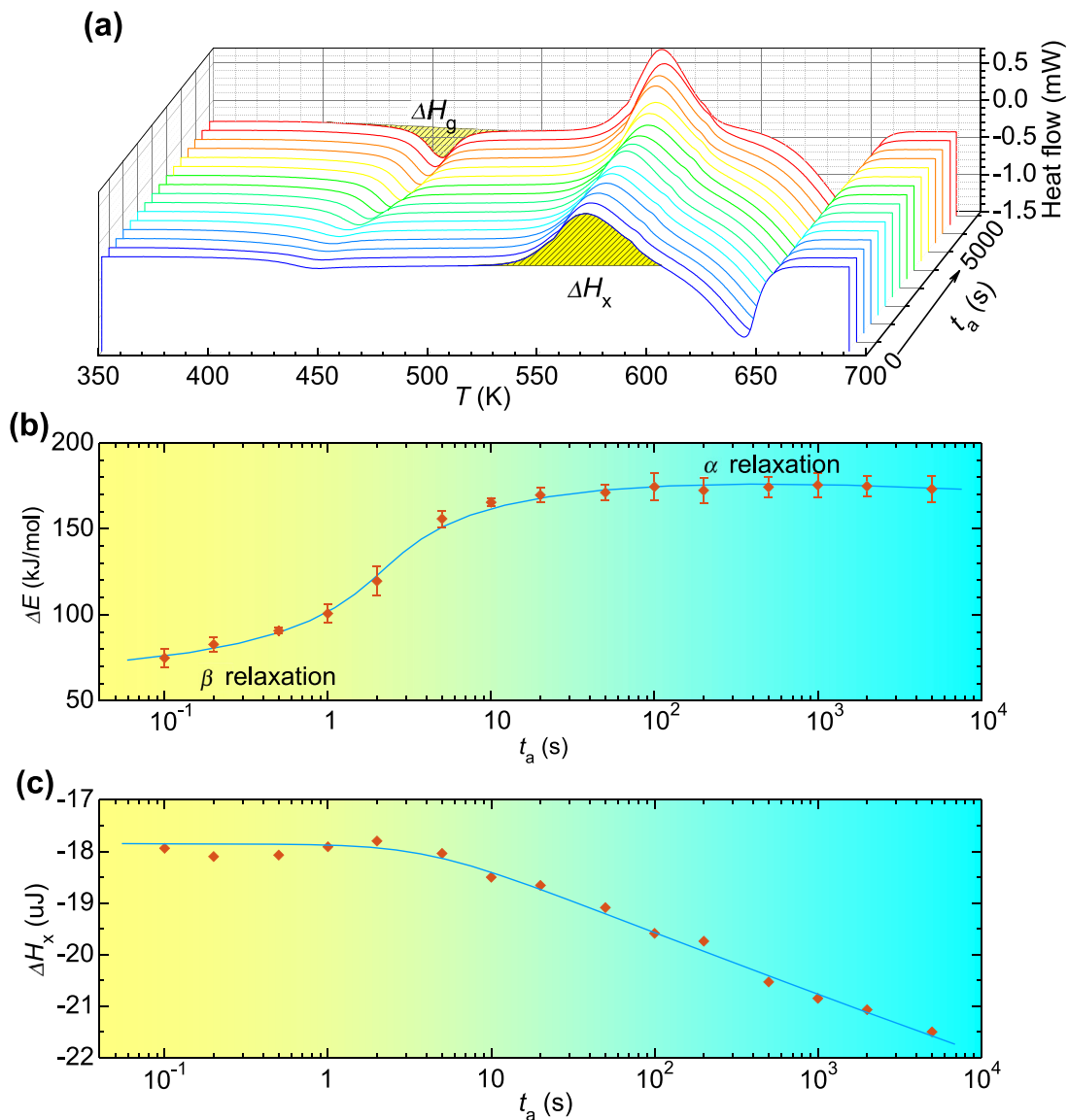


Fig. 4. The crystallization of relaxed metallic glasses. (a) The heat flows of the glass upon subsequent heating $R_h=1500$ K/s after being annealed at $T_a=383$ K for various times. The relaxation enthalpy (ΔH_g) and crystallization enthalpy (ΔH_x) are highlighted by shading. (b) The evolution of relaxation barrier (ΔE) along with the annealing time during annealing at $T_a=383$ K. (c) The crystallization enthalpy (ΔH_x) versus the annealing time.

relaxation stage, the enthalpy for the fast-cooled sample changes by about 0.4 kJ/mol, while that for the slow-cooled sample changes by about 0.15 kJ/mol. In contrast, the enthalpy changes the same for the two metallic glasses during the α relaxation stage. In this way, the amount of β relaxation can be evaluated by the enthalpy variation during β relaxation (H_β).

Fig. 5(b) shows the correlation between the crystallization fraction and the amount of β relaxation. The metallic glass cooled at a higher rate exhibits more β relaxation and is more difficult to crystallize than the glass cooled at a lower rate. It has been observed that the β relaxation corresponds to the string-like motions of small atoms [37], which may survive in the supercooled liquid. Schematic microstructures are proposed to illustrate the structural evolution along with cooling rate, as shown in the inset images in Fig. 5(b). The one-dimensional orange structures represent the structure with β relaxation motion, while the blue zones represent the structure with a more dense packing structure that favors crystallization.

4. Discussion

In order to understand the kinetic behavior displayed in Fig. 3 it is necessary to consider two effects that are related to the melt quenching process: a retained cluster distribution and the β relaxation. In this case it is noted that the 1600 K/s cooling rate has been established as the critical cooling rate to achieve a glass. At lower cooling rates crystallization develops during quenching. Thus, at 1600 K/s the cluster size distribution that develops during cooling is not sufficient to achieve the critical size for crystal nucleation, but can be retained in the glass as noted by Schawe and Löffler [38] and Xie et al. [39]. Similarly, at the 10,000 K/s cooling rate some cluster distribution develops and can be retained, but the size range is smaller than that for the 1600 K/s cooling rate due to the reduced time available for cluster evolution. Upon reheating the glass cluster evolution to the critical size is governed by sluggish diffusion at low temperature and the TTT curves for both the 1600 K/s and the 10,000 K/s cooling rates overlap. The

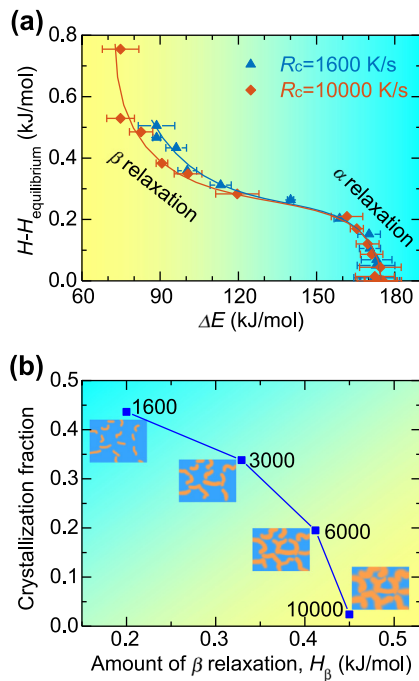


Fig. 5. The correlation between crystallization fraction and the amount of β relaxation. (a) The excess enthalpy of glass relative to the equilibrium supercooled liquid state versus ΔE . The initial decrease in enthalpy is mainly attributed to β relaxation where the enthalpy decreases by about 0.45 kJ/mol for the fast-cooled glass and about 0.2 kJ/mol for the slow-cooled glass. The enthalpy variation caused by α relaxation is about 0.2 kJ/mol for both glasses. (b) The crystallization fraction is measured upon heating at 4000 K/s (referred to Fig. 2(c)) for the metallic glasses cooled at 1600 K/s, 3000 K/s, 6000 K/s and 10,000 K/s. The amount of β relaxation is determined by the enthalpy change during β relaxation (referred to Fig. 4(e)). Inset images illustrate schematically the evolution of microstructure. The orange zones represent the structure for β relaxation. (For interpretation of the references to colour in this figure legend, the reader is referred to the web version of this article).

TTT curves begin to depart from overlap since the critical size increases with increasing temperature so that the retained clusters at the 10,000 K/s cooling rate fall below the critical size and require additional time to reach the nucleation onset. For the 1600 K/s cooling rate the retained clusters are larger and can act to promote nucleation at temperatures above the overlap departure. At the same time the increased amount of β relaxation for the glass cooled at 10,000 K/s acts to retard the onset of nucleation more than for the glass cooled at 1600 K/s. Thus, the β relaxation effect acts in an opposite way to the retained cluster distribution in influencing nucleation. A full kinetics analysis must consider both effects that is beyond the scope of the present work.

The α relaxation exists over wide temperatures ranges (from glass to supercooled liquid) and is correlated with the crystal growth and the atomic diffusion. However, it is known that the β relaxation vanishes in supercooled liquid or merges with α relaxation. Our findings suggest that the β relaxation can also survive from glass to supercooled liquid at high temperatures and is correlated with the nucleation of crystals. The finding that the state of glass has an important role in modulating the nucleation kinetics of the supercooled liquid has promising potential applications for promoting the applications of thermal plastic deformation of metallic glasses in supercooled liquid region.

5. Conclusions

In summary, the phase transition kinetics of an Au-based metallic glass-forming system is studied using the high-precision fast

differential scanning calorimeter. Phase existence region diagrams are determined upon cooling and heating. It is found that the fast-cooled metallic glass is more difficult to crystallize. This is attributed to the activation of β relaxation that can depress the crystal nucleation. The correlation between the two intrinsic metastable characters suggests a promising route for enhancing the stability of supercooled liquid by modulating the characters of glasses.

Declaration of Competing Interest

The authors declare that they have no known competing financial interests or personal relationships that could have appeared to influence the work reported in this paper.

Acknowledgments

The financial supports from National Key R&D Program of China (2018YFA0703604, 2018YFA0703602), National Natural Science Foundation of China (NSFC 51922102, 51827801, 51771216), Zhejiang Provincial Natural Science Foundation of China (LR18E010002, LY17E010005) are acknowledged. M.G. and J.H.P. gratefully acknowledge the support of the U.S. Office of Naval Research (ONR N00014-16-1-2401).

Supplementary materials

Supplementary material associated with this article can be found, in the online version, at doi:10.1016/j.actamat.2019.11.063.

References

- [1] S.V. Ketov, Y.H. Sun, S. Nachum, Z. Lu, A. Checchi, A.R. Beraldin, H.Y. Bai, W.H. Wang, D.V. Louzguine-Luzgin, M.A. Carpenter, A.L. Greer, Rejuvenation of metallic glasses by non-affine thermal strain, *Nature* 524 (2015) 200–203.
- [2] Y.C. Hu, Y.Z. Wang, R. Su, C.R. Cao, F. Li, C.W. Sun, Y. Yang, P.F. Guan, D.W. Ding, Z.L. Wang, W.H. Wang, A highly efficient and self-stabilizing metallic-glass catalyst for electrochemical hydrogen generation, *Adv. Mater.* 28 (2016) 10293–10297.
- [3] A. Hirata, L.J. Kang, T. Fujita, B. Klumov, K. Matsue, M. Kotani, A.R. Yavari, M.W. Chen, Geometric frustration of icosahedron in metallic glasses, *Science* 341 (2013) 376–379.
- [4] W.L. Johnson, G. Kaltenboeck, M.D. Demetriou, J.P. Schramm, X. Liu, K. Samwer, C.P. Kim, D.C. Hofmann, Beating crystallization in glass-forming metals by millisecond heating and processing, *Science* 332 (2011) 828–833.
- [5] J. Plummer, W.L. Johnson, Is metallic glass poised to come of age? *Nat. Mater.* 14 (2015) 553–555.
- [6] J.Q. Wang, Y.H. Liu, M.W. Chen, G.Q. Xie, D.V. Louzguine-Luzgin, A. Inoue, J.H. Perepezko, Rapid degradation of Azo dye by Fe-based metallic, *Adv. Funct. Mater.* 22 (2012) 2567–2570.
- [7] D.C. Hofmann, J.Y. Suh, A. Wiest, G. Duan, M.L. Lind, M.D. Demetriou, W.L. Johnson, Designing metallic glass matrix composites with high toughness and tensile ductility, *Nature* 451 (2008) 1085–1089.
- [8] W.L. Song, Y. Wu, H. Wang, X.J. Liu, H.W. Chen, Z.X. Guo, Z.P. Lu, Microstructural control via copious nucleation manipulated by in situ formed nucleants: large-sized and ductile metallic glass composites, *Adv. Mater.* 28 (2016) 8156–8161.
- [9] A. Takeuchi, Y. Zhang, K. Takenaka, A. Makino, Thermodynamic analysis of binary Fe₈₅B₁₅ to quinary Fe₈₅Si₂B₈P₄Cu₁ alloys for primary crystallizations of α -Fe in nanocrystalline soft magnetic alloys, *J. Appl. Phys.* 117 (2015) 17B737.
- [10] P.P. Wang, J.Q. Wang, J.T. Huo, W. Xu, X.M. Wang, G. Wang, Fast degradation of Azo dye by nanocrystallized Fe-based alloys, *Sci. China Phys. Mech. Astron.* 60 (2017) 076112.
- [11] S.Q. Chen, G.N. Yang, S.T. Luo, S.J. Yin, J.L. Jia, Z. Li, S.H. Gao, Y. Shao, K.F. Yao, Unexpected high performance of Fe-based nanocrystallized ribbons for azo dye decomposition, *J. Mater. Chem. A* 5 (2017) 14230–14240.
- [12] G. Sun, J. Xu, P. Harrowell, The mechanism of the ultrafast crystal growth of pure metals from their melts, *Nat. Mater.* 17 (2018) 881–886.
- [13] M. Salinga, B. Kersting, I. Ronneberger, V.P. Jonnalagadda, X.T. Vu, M. Le Gallo, I. Giannopoulos, O. Cojocaru-Miredin, R. Mazzarello, A. Sebastian, Monatomic phase change memory, *Nat. Mater.* 17 (2018) 681–685.
- [14] C. Desgranges, J. Delhommelle, Unusual crystallization behavior close to the glass transition, *Phys. Rev. Lett.* 120 (2018) 115701.
- [15] C.G. Tang, P. Harrowell, Anomalously slow crystal growth of the glass-forming alloy CuZr, *Nat. Mater.* 12 (2013) 507–511.
- [16] A.L. Greer, Crystallization of amorphous alloys, *Metall. Mater. Trans. A* 27 (1996) 549–555.

- [17] M.L. Wang, K. Zhang, Z.S. Li, Y.H. Liu, J. Schroers, M.D. Shattuck, C.S. O'Hern, Asymmetric crystallization during cooling and heating in model glass-forming systems, *Phys. Rev. E* 91 (2015) 032309.
- [18] J. Schroers, Y. Wu, R. Busch, W.L. Johnson, Transition from nucleation controlled to growth controlled crystallization in Pd₄₃Ni₁₀Cu₂₇P₂₀ melts, *Acta Mater* 49 (2001) 2773–2781.
- [19] J. Schroers, A. Masuhr, W.L. Johnson, R. Busch, Pronounced asymmetry in the crystallization behavior during constant heating and cooling of a bulk metallic glass-forming liquid, *Phys. Rev. B* 60 (1999) 11855–11858.
- [20] S. Pogatscher, P.J. Uggowitzer, J.F. Löffler, In-situ probing of metallic glass formation and crystallization upon heating and cooling via fast differential scanning calorimetry, *Appl. Phys. Lett.* 104 (2014) 251908.
- [21] H.B. Yu, W.H. Wang, H.Y. Bai, K. Samwer, The β -relaxation in metallic glasses, *Nat. Sci. Rev.* 1 (2014) 429–461.
- [22] A. Hirata, N. Kawahara, Y. Hirotsu, A. Makino, Local structure changes on annealing in an Fe–Si–B–P bulk metallic glass, *Intermetallics* 17 (2009) 186–189.
- [23] L. Xue, W.M. Yang, H.S. Liu, H. Men, A.D. Wang, C.T. Chang, B.L. Shen, Effect of Co addition on the magnetic properties and microstructure of FeNbCu nanocrystalline alloys, *J. Magn. Magn. Mater.* 419 (2016) 198–201.
- [24] L.J. Song, W. Xu, J.T. Huo, J.Q. Wang, X.M. Wang, R.W. Li, Two-step relaxations in metallic glasses during isothermal annealing, *Intermetallics* 93 (2018) 101–105.
- [25] P. Luo, P. Wen, H.Y. Bai, B. Ruta, W.H. Wang, Relaxation decoupling in metallic glasses at low temperatures, *Phys. Rev. Lett.* 118 (2017) 225901.
- [26] J.C. Qiao, Y.-J. Wang, L.Z. Zhao, L.H. Dai, D. Crespo, J.M. Pelletier, L.M. Keer, Y. Yao, Transition from stress-driven to thermally activated stress relaxation in metallic glasses, *Phys. Rev. B* 94 (2016) 104203.
- [27] J.H. Perepezko, T.W. Glendinning, J.Q. Wang, Nanocalorimetry measurements of metastable states, *Thermochim. Acta* 603 (2015) 24–28.
- [28] M. Kobayashi, H. Tanaka, The reversibility and first-order nature of liquid–liquid transition in a molecular liquid, *Nat. Commun.* 7 (2016) 13438.
- [29] J.Q. Wang, Y. Shen, J.H. Perepezko, M.D. Ediger, Increasing the kinetic stability of bulk metallic glasses, *Acta Mater.* 104 (2016) 25–32.
- [30] S. Pogatscher, D. Leutenegger, J.E.K. Schawe, P.J. Uggowitzer, J.F. Löffler, Solid–solid phase transitions via melting in metals, *Nat. Commun.* 7 (2016) 11113.
- [31] Z. Evenson, S.E. Naleway, S. Wei, O. Gross, J.J. Kruzic, I. Gallino, W. Possart, M. Stommel, R. Busch, β relaxation and low-temperature aging in a Au-based bulk metallic glass: From elastic properties to atomic-scale structure, *Phys. Rev. B* 89 (2014) 174204.
- [32] B. Ruta, Y. Chushkin, G. Monaco, L. Cipelletti, E. Pineda, P. Bruna, V.M. Giordano, M. Gonzalez-Silveira, Atomic-scale relaxation dynamics and aging in a metallic glass probed by x-ray photon correlation spectroscopy, *Phys. Rev. Lett.* 109 (2012) 165701.
- [33] D.R. Uhlmann, A kinetic treatment of glass formation, *J. Non-Cryst. Solids* 7 (1972) 337–348.
- [34] J.M. Pelletier, S. Cardinal, J.C. Qiao, M. Eisenbart, U.E. Klotz, Main and secondary relaxations in an Au-based bulk metallic glass investigated by mechanical spectroscopy, *J. Alloys Compd.* 684 (2016) 530–536.
- [35] C. Zhou, Y.Z. Yue, L.N. Hu, Revealing the connection between the slow β relaxation and sub- T_g enthalpy relaxation in metallic glasses, *J. Appl. Phys.* 120 (2016) 225110.
- [36] B.G. Zhao, B. Yang, A.S. Abyzov, J.W.P. Schmelzer, J. Rodriguez-Viejo, Q.J. Zhai, C. Schick, Y.L. Gao, Beating homogeneous nucleation and tuning atomic ordering in glass-forming metals by nanocalorimetry, *Nano Lett.* 17 (2017) 7751–7760.
- [37] H.B. Yu, R. Richert, K. Samwer, Structural rearrangements governing Johari–Goldstein relaxations in metallic glasses, *Sci. Adv.* 3 (2017) e1701577.
- [38] J.E.K. Schawe, J.F. Löffler, Existence of multiple critical cooling rates which generate different types of monolithic metallic glass, *Nat. Commun.* 10 (2019) 1337.
- [39] Y.J. Xie, S. Sohn, M.L. Wang, H.L. Xin, Y. Jung, M.D. Shattuck, C.S. O'Hern, J. Schroers, J.J. Cha, Supercluster-coupled crystal growth in metallic glass forming liquids, *Nat. Commun.* 10 (2019) 915.